A Facile Vapor−Phase Hydrothermal Method for Direct Growth of Titanate Nanotubes on a Titanium Substrate via a Distinctive Nanosheet Roll−Up Mechanism

ARTICLE *in* JOURNAL OF THE AMERICAN CHEMICAL SOCIETY · NOVEMBER 2011

Impact Factor: 12.11 · DOI: 10.1021/ja207530e · Source: PubMed

8 AUTHORS, INCLUDING:

Porun Liu
Griffith University
78 PUBLICATIONS **1,125** CITATIONS
SEE PROFILE

Haimin Zhang
Griffith University
97 PUBLICATIONS **1,339** CITATIONS
SEE PROFILE

Shanqing Zhang
Griffith University
121 PUBLICATIONS **2,749** CITATIONS
SEE PROFILE

Huijun Zhao
Griffith University
307 PUBLICATIONS **6,139** CITATIONS
SEE PROFILE

JACS
JOURNAL OF THE AMERICAN CHEMICAL SOCIETY

COMMUNICATION

pubs.acs.org/JACS

A Facile Vapor-Phase Hydrothermal Method for Direct Growth of Titanate Nanotubes on a Titanium Substrate via a Distinctive Nanosheet Roll-Up Mechanism

Porun Liu,[†] Haimin Zhang,[†] Hongwei Liu,[†] Yun Wang,[†] Xiangdong Yao,[‡] Guangshan Zhu,[‡] Shanqing Zhang,[†] and Huijun Zhao*[,†]

[†]Centre for Clean Environment and Energy and Griffith School of Environment, Griffith University, Gold Coast Campus, QLD 4222, Australia

[‡]QLD Micro- and Nanotechnology Centre, Griffith University, Nathan Campus, QLD 4111, Australia

Supporting Information

ABSTRACT: We present a facile vapor-phase hydrothermal approach for direct growth of vertically aligned titanate nanotubes on a titanium foil substrate. The resultant nanotubes display external diameters of 50−80 nm and walls with an average thickness of 10 nm that consist of more than 10 titanate layers. This is in strong contrast to the titanate nanotubes obtained from alkaline liquid-phase hydrothermal methods, which are generally smaller than 12 nm in external diameter and have walls consisting of less than five titanate layers. Importantly, the investigation confirmed that under vapor-phase hydrothermal conditions, the nanotubes were formed via a distinctive nanosheet roll-up mechanism that differs remarkably from those of conventional liquid-phase hydrothermal processes. For the first time, a coaxial circular cylinder crystal structure of the resultant nanotubes was confirmed.

Titanium oxide nanotubes have received considerable attention because of their superior electron transport properties, high aspect ratio, and photocatalytic activities, which are advantageous for photocatalysis, energy conversion and storage, biomedicine, and sensing applications.[1−8] Over the past two decades, many synthetic methods, including template-assisted approaches, anodization, seeded growth, and liquid-phase hydrothermal methods (LPH) have been reported.[9−12] Among them, LPH methods have been the most widely used to obtain large quantities of titanate nanotubes.[11,13] To date, all titanate nanotubes obtained from LPH processes are almost exclusively in the solution suspension or precipitate forms.[11,13,14] Regardless of the synthesis conditions, all reported titanate nanotubes synthesized using alkaline LPH methods possess similar diameters of 8−12 nm.[11,13−15] To the best of our knowledge, no vapor-phase hydrothermal (VPH) method for the synthesis of titanate nanotubes has been reported to date. In regard to titanate nanotube formation mechanisms under LPH conditions, although a variety of different views have been proposed, the precise formation mechanism is still somewhat controversial because of the lack of direct experimental evidence in support.[13,16,17] The extremely small size of the tubular structures partially contributes to the difficulties in obtaining direct experimental evidence to confirm the proposed formation mechanisms.[16−19] For the same reason, the precise crystal structures of hydrothermally produced nanotubes have not been identified.

Herein we report for the first time a facile VPH method for direct growth of vertically aligned titanate nanotubes with larger diameters on a titanium foil substrate via a distinctive nanosheet roll-up mechanism. Unlike the titanate nanotubes obtained from LPH processes, the diameters of the titanate nanotubes obtained from VPH processes are much larger and tunable. Importantly, the nanosheet formation, roll-up, and subsequent crystal reformation processes here are clearly demonstrated by experimental evidence that categorically confirms the proposed nanosheet roll-up mechanism. The resultant nanotubes possess a coaxial circular cylinder crystal structure.

For a typical VPH synthesis process, a titanium foil substrate coated with NaOH is hydrothermally treated in an autoclave with the vapor generated from a 28% ammonia solution at 150 °C for 1−72 h (Scheme S1 in the Supporting Information). Figure 1a shows a typical surface scanning electron microscopy (SEM) image of the as-synthesized sample after 24 h of VPH reaction. It reveals a vertically aligned nanotubular structure formed on the titanium foil substrate (Figure 1a and Figure S1). The as-synthesized nanotubes had external diameters of 50−80 nm and lengths of several hundred nanometers. The nanotubes were further examined by the transmission electron microscopy (TEM), as shown in Figure 1b. The TEM image shows that the internal and external diameters of the examined nanotube are about 30 and 50 nm, respectively (Figure 1b). The high-resolution TEM (HRTEM) image (Figure 1c) reveals that the spacing between adjacent layers of the nanotube wall is 7.7 Å and that the nanotube wall has a thickness of 10 nm and consists of 13 titanate layers (Figure 1c). X-ray diffraction (XRD) analysis and Raman spectra of the as-synthesized nanotubes obtained using VPH and LPH methods are given in Figure S2. As expected, the XRD data confirm that the nanotubes fabricated by these two methods possess similar crystal structures (Figure S2a).[20−23] The results obtained from diffraction data (Table S1), Raman spectra (Figure S2b), energy-dispersive X-ray spectroscopy (EDXS) (Figure S3a), and X-ray photoelectron spectroscopy (XPS) (Figure S3b,c) confirm that the structure of the as-synthesized nanotubes can

Received: August 10, 2011
Published: October 28, 2011

dx.doi.org/10.1021/ja207530e | *J. Am. Chem. Soc.* 2011, 133, 19032–19035

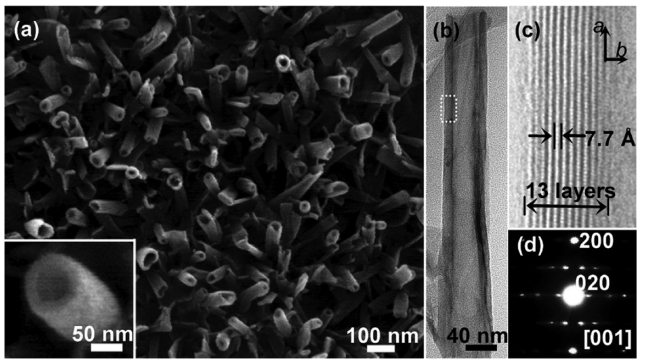

Figure 1. Morphological and structural properties of the as-synthesized titanate nanotubes on a Ti foil substrate after VPH reaction at 150 °C for 24 h: (a) SEM image; (b) TEM image; (c) HRTEM image; (d) SAED pattern. The inset in (a) is a high-magnification SEM image of a resultant nanotube.

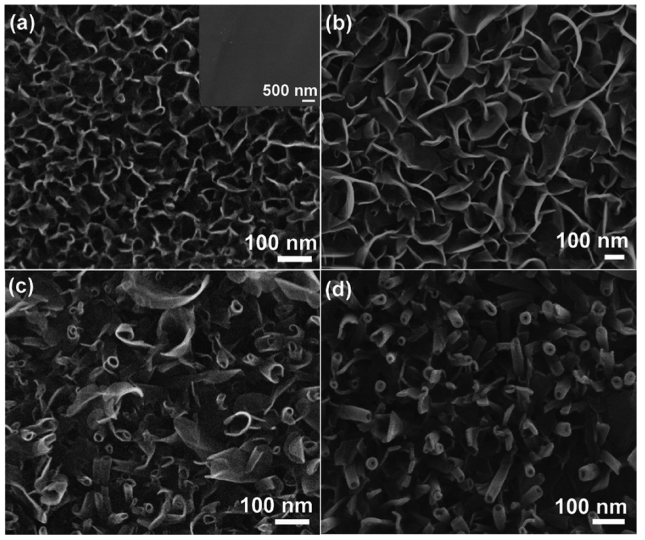

Figure 2. SEM images of the nanostructures grown using the VPH treatment process for (a) 3, (b) 6, (c) 12, and (d) 72 h. The inset in (a) is an SEM image of the original Ti foil.

be assigned as an orthorhombic lepidocrocite-type titanate, represented by $H_{0.7-x-y}Na_x(NH_4)_yTi_{1.825}\square_{0.175}O_4 \cdot H_2O$ (where $\square$ = vacancy), which is a cation-exchanged product of $H_{0.7}Ti_{1.825}\square_{0.175}O_4 \cdot H_2O$.[20−23] A selected-area electron diffraction (SAED) pattern of the nanotube wall is given in Figure 1d. It was taken with the incident beam along the [001] direction, indicating that the multilayered nanotube was rolled in the [001] direction with the tubular axis along the [100] direction. It is well-known that typical titanate nanotubes made from the alkaline LPH method normally display an external diameter of less than 12 nm with a nanotube wall consisting of less than five titanate layers (Figure S4).[11,13,16,24] Although the nanotubes produced by the LPH and VPH methods show similar crystal characteristics (Figure S2), the VPH-produced nanotubes are 5 times larger in diameter and nearly 3 times thicker in nanotube walls relative to the LPH-produced titanate nanotubes (Figure 1b,c). Such significant dimensional differences could be ascribed to the remarkable differences in growth environment and formation mechanisms of the two methods.

To study the nanotube formation mechanism under VPH conditions, the structure growth processes on the titanium foil substrate were examined by SEM. Figure 2 shows SEM images of the as-synthesized samples for different durations of VPH treatment. Before VPH treatment, no structures could be observed on the surface of the pretreatment titanium foil (Figure 2a inset). A thin-liquid-layer alkaline environment on the substrate surface was instantly established during the initial stage of the VPH process via the wetting of the precoated NaOH by the condensed NH_3-saturated water vapor. Dissolution of the titanium substrate by NaOH then took place, similar to the case of the alkaline LPH process. However, the structure formation (precipitation) under VPH conditions could be more rapid than in the LPH process. This is because of the small solution volume and high initial NaOH concentration in a typical VPH process. The entire thin liquid layer can be rapidly supersaturated by the titanate species from the dissolution of the titanium substrate. This is in strong contrast to an alkaline LPH process, where the titanate species from the dissolution of titanium substrate diffuse into the bulk solution. The concentration of the titanate species must first reach saturation in the bulk solution, then the structure formation may occur at locations where the concentrations of the titanate species are higher than the saturation concentration (resulting from the continued dissolution process).

After 3 h of VPH treatment, vertically aligned nanosheets similar to those obtained by LPH method[25] were formed on the titanium foil substrate (Figure 2a). The nanosheets were grown to significantly larger sizes when the reaction time was increased to 6 h (Figure 2b). At this stage of VPH treatment, the average thickness of the as-synthesized nanosheets was found to be ~10 nm. No significant changes in the nanosheets' dimensions (in terms of thickness and area) were observed when the reaction time was further increased. This can be attributed to the dramatically decreased NaOH concentration in the thin liquid layer. Unlike the case of an alkaline LPH process, where the dissolution of titanium can be sustained by continuously supplying NaOH from the bulk solution, the dissolution of titanium cannot be sustained once the limited amount of precoated NaOH is consumed, as the alkalinity provided by the NH_3-saturated water vapor is insufficient to dissolve the titanium metal rapidly. This means that the alkalinity within the reaction zone changes dramatically over time, which could lead to different formation mechanisms at different stages of the VPH process; this is one of the distinctive differences between the LPH and VPH methods. Indeed, the SEM images of the VPH-treated samples obtained at longer treatment times indicate a distinctive nanosheet roll-up process. Figure 2c shows a typical SEM image obtained from an as-synthesized sample after 12 h of VPH treatment. A noticeable amount of matured nanotubes and half-rolled nanosheets are displayed. At this stage of the VPH process, the precoated NaOH is exhausted, and the reaction environment is dominated by the NH_3-saturated water vapor. The precise driving force for the roll-up of the nanosheets is still unclear. However, the obtained results suggest that the interaction of the nanosheets with NH_3 molecules plays a key role in creating the surface tension leading to the curvature of the multilayered structure.[26−28] The critical role of NH_3 in the nanosheet roll-up is supported by the results shown in Figure S5. These experiments were performed in absence of NH_3, with the other conditions kept identical to the VPH conditions employed in Figure 1. Nanosheets were obtained for all cases, but no nanosheets were obviously rolled-up to form nanotubes.

dx.doi.org/10.1021/ja207530e |J. Am. Chem. Soc. 2011, 133, 19032–19035

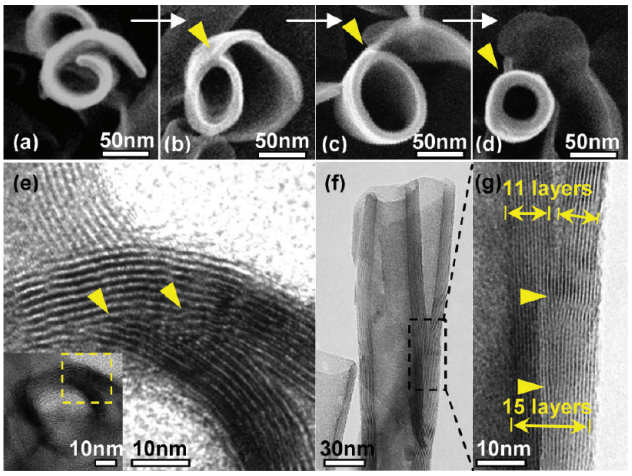

Figure 3. (a–d) top-view SEM images of the morphological evolution from a nanosheet into a nanotube; (e) TEM image of a joint of a scrolled nanosheet viewed along the scroll axis; (f) side-view TEM image of a nanotube with an undetached exfoliating nanosheet; (g) magnified TEM image of the dashed-square region in (f).

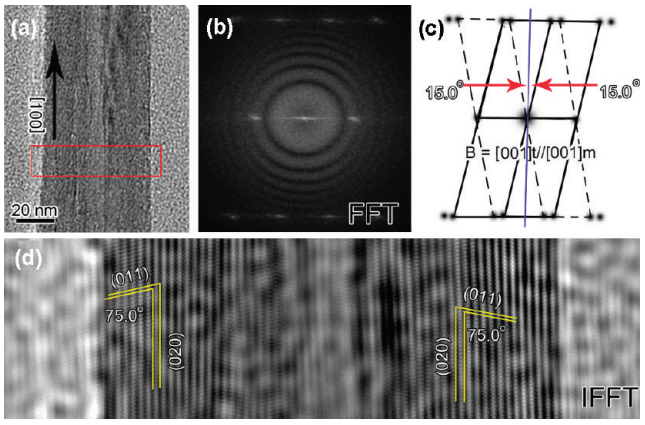

Figure 4. (a) TEM image of an individual titanate nanotube. (b) FFT image of the nanotube walls. (c) Schematic FFT graph deduced from (b). (d) IFFT image corresponding to the area marked in red in (a).

The formation of nanosheets was due to the presence of precoated NaOH. After 24 h of VPH treatment, all of the 2D nanosheets were rolled up to form vertically aligned 1D nanotubes (Figure 1a). No noticeable structural or morphological changes were observed when the treatment time was extended to 72 h (Figure 2d).

To gain insight into the nanosheet roll-up and structural evolution processes, high-magnification SEM and TEM images of the sample obtained after 18 h of VPH treatment were taken. At this VPH stage, the sample consists of morphologies of infant and mature nanotubes (Figure S6). The roll-up process is illustrated by distinct rolling stages of individual nanosheets or nanotubes, as presented in Figure 3a–d. Figure 3a shows a rolled-up titanate nanosheet before nanotube formation. In the subsequent step shown in Figure 3b, one end of the rolled nanosheet joins to its intrados in the middle part by saturating the dangling bonds of the nanosheet,[29] as indicated by the arrow. The TEM image of the joining section viewed from the tube axis is given in Figure 3e. It clearly shows that the second, third, and fourth inner layers of the joining end are merged at the same host layer, namely, the second inner layer of the intrados, as indicated by the left arrow, while other layers undergo the merging (crystal reformation) process,[30,31] as shown by the right arrow. This indubitably not only demonstrates that the joining process involves a physically rolled-up nanosheet but also shows that the crystal reformation at the joint plays a decisive role in completing the nanotube formation. The excess segment of the nanosheet is detached to form a mature nanotube when the crystal reformation (merging) process is completed. The detachment of the excess segment was initiated from the top rim of the joint, as shown by the arrow in Figure 3c. Figure 3d shows a nearly mature nanotube at the late stage of the detachment process. TEM images of the detaching segment (Figure 3f,g) show a "Y"-shaped junction with 11 layers on the branches and 15 layers on the joint. The results shown in Figure 3e–g are more clearly illustrated by the schematic diagram shown in Scheme S2. It should be noted that the circularity of the nanotubular structure improved from an elliptical shape (Figure 3b) to a circular shape (Figure 3d) as viewed along the tube axis because of the even elastic strain distribution along the tubular cylinder wall after the establishment of the orbicular multilayered structure.

The results presented above demonstrate that the titanate nanotubes obtained under the VPH conditions are formed by direct roll-up of entire nanosheets and crystal reformation at the joint. If this is true, then the resultant nanotube should possess a seamless circular crystal structure. In other words, the multilayered walls on both sides of the nanotube should be symmetrical and identical in crystal structure. Figure 4a shows a TEM image of an individual titanate nanotube after 24 h of reaction. Figure 4b shows the fast Fourier transform (FFT) image on both sides of the nanotube walls corresponding to the area marked in red in Figure 4a. The schematic FFT graph deduced from Figure 4b shows a symmetric FFT image with an identical (110) to (020) planar angle of 75°. This was further confirmed by the inverse-FFT (IFFT) images shown in Figure 4d, where the measured angles between the (110) and (020) planes on both sides of the nanotube walls were identical. This confirms that the crystal structure of the titanate nanotube produced under VPH conditions is indeed in the form of a coaxial circular cylinder.

In comparison with the nanotubes obtained under alkaline LPH conditions, the nanotubes obtained in this work under VPH conditions possess much larger diameters and wall thicknesses. The formation mechanisms also differ remarkably between the two methods. These results may be attributed to the following key differences between the two methods. The dissolved titanate species undergo the physical and chemical reformation processes in solution to form the basic building blocks (precursors). The dimensional and structural properties of the basic building blocks are important attributes that strongly influence the nanostructure formation. These properties are determined by the physiochemical reformation conditions. In the case of the alkaline LPH process, the reformation occurs mainly in the bulk solution under an essentially constant NaOH concentration (alkalinity) for a reasonably long period. However, reformation conditions are distinctively different in the VPH process because the entire thin liquid layer (the reaction zone) is rapidly supersaturated by the dissolved titanate species, allowing only a short time for the reformation process before precipitation occurs. This could mean that the basic building blocks produced by the two methods are vastly different, resulting in different sizes of nanostructures. With the LPH process, the dissolved titanate species

are highly mobile within the large volume of the bulk solution. Under such conditions, the resultant nanotubes possess high aspect ratios, and seed-formation-oriented crystal growth would be the most likely formation mechanism.[17,24,32] In contrast, the mobility of the dissolved titanate species is low under the VPH conditions. As a result, the production and consumption of the titanate species are highly localized. This adds to the changes in reaction environment with time (caused by the decreasing NaOH concentration in the thin liquid layer), leading to a two-step formation mechanism. The nanosheets are first formed in the presence of sufficient concentration of NaOH. This is followed by the nanosheet roll-up and crystal reformation processes driven by the NH_3-saturated water vapor to form nanotubes.

In summary, we have demonstrated a facile VPH method for the direct growth of vertically aligned titanate nanotubes on a titanium metal foil substrate. These nanotubes have large diameters of 50−80 nm that cannot be obtained using the conventional alkaline LPH method, and this can be attributed to the unique hydrothermal environment created by the NH_3-saturated water vapor phase. More importantly, we have proposed and experimentally validated for the first time a distinctive nanosheet roll-up/crystal reformation mechanism for formation of nanotubes under VPH conditions. A seamless coaxial circular crystal tubular structure has also been proposed and experimentally validated. We believe the findings presented in this work advance the knowledge of nanotube formation mechanisms and could be extended to the fabrication of other metal oxides on desirable substrates for wider applications.

■ ASSOCIATED CONTENT

Supporting Information. Experimental details; cross-sectional SEM image, XRD data, and Raman, EDXS, and XPS spectra of the titanate nanotubes; SEM image of titanate nanotubes prepared using the LPH method; SEM images of samples prepared for 18 h and those without ammonia atmosphere; and a schematic illustration of the crystal reformation process during nanotube growth. This material is available free of charge via the Internet at http://pubs.acs.org.

■ AUTHOR INFORMATION

Corresponding Author
h.zhao@griffith.edu.au

■ ACKNOWLEDGMENT

This work was financially supported by the Australian Research Council.

■ REFERENCES

(1) Fujishima, A.; Honda, K. *Nature* **1972**, *238*, 37.
(2) Schmidt, O. G.; Eberl, K. *Nature* **2001**, *410*, 168.
(3) Varghese, O. K.; Paulose, M.; Grimes, C. A. *Nat. Nanotechnol.* **2009**, *4*, 592.
(4) Armstrong, A. R.; Armstrong, G.; Canales, J.; García, R.; Bruce, P. G. *Adv. Mater.* **2005**, *17*, 862.
(5) Macak, J. M.; Zlamal, M.; Krysa, J.; Schmuki, P. *Small* **2007**, *3*, 300.
(6) Chopra, N. G.; Luyken, R. J.; Cherrey, K.; Crespi, V. H.; Cohen, M. L.; Louie, S. G.; Zettl, A. *Science* **1995**, *269*, 966.
(7) Song, Y.-Y.; Schmidt-Stein, F.; Bauer, S.; Schmuki, P. *J. Am. Chem. Soc.* **2009**, *131*, 4230.
(8) Jiang, Z.; Yang, F.; Luo, N.; Chu, B. T. T.; Sun, D.; Shi, H.; Xiao, T.; Edwards, P. P. *Chem. Commun.* **2008**, 6372.
(9) Mor, G. K.; Varghese, O. K.; Paulose, M.; Shankar, K.; Grimes, C. A. *Sol. Energy Mater. Sol. Cells* **2006**, *90*, 2011.
(10) Lakshmi, B. B.; Patrissi, C. J.; Martin, C. R. *Chem. Mater.* **1997**, *9*, 2544.
(11) Kasuga, T.; Hiramatsu, M.; Hoson, A.; Sekino, T.; Niihara, K. *Langmuir* **1998**, *14*, 3160.
(12) Yue, L.; Gao, W.; Zhang, D.; Guo, X.; Ding, W.; Chen, Y. *J. Am. Chem. Soc.* **2006**, *128*, 11042.
(13) Kasuga, T.; Hiramatsu, M.; Hoson, A.; Sekino, T.; Niihara, K. *Adv. Mater.* **1999**, *11*, 1307.
(14) Wang, N.; Lin, H.; Li, J.; Zhang, L.; Lin, C.; Li, X. *J. Am. Ceram. Soc.* **2006**, *89*, 3564.
(15) Bavykin, D. V.; Friedrich, J. M.; Walsh, F. C. *Adv. Mater.* **2006**, *18*, 2807.
(16) Yao, B. D.; Chan, Y. F.; Zhang, X. Y.; Zhang, W. F.; Yang, Z. Y.; Wang, N. *Appl. Phys. Lett.* **2003**, *82*, 281.
(17) Kukovecz, A.; Hodos, M.; Horvath, E.; Radnoczi, G.; Konya, Z.; Kiricsi, I. *J. Phys. Chem. B* **2005**, *109*, 17781.
(18) Wu, D.; Liu, J.; Zhao, X.; Li, A.; Chen, Y.; Ming, N. *Chem. Mater.* **2006**, *18*, 547.
(19) Bavykin, D. V.; Parmon, V. N.; Lapkin, A. A.; Walsh, F. C. *J. Mater. Chem.* **2004**, *14*, 3370.
(20) Ma, R.; Sasaki, T.; Bando, Y. *Chem. Commun.* **2005**, 948.
(21) Ma, R.; Fukuda, K.; Sasaki, T.; Osada, M.; Bando, Y. *J. Phys. Chem. B* **2005**, *109*, 6210.
(22) Mao, Y.; Wong, S. S. *J. Am. Chem. Soc.* **2006**, *128*, 8217.
(23) Gao, T.; Wu, Q.; Fjellvåg, H.; Norby, P. *J. Phys. Chem. C* **2008**, *112*, 8548.
(24) Zhang, H.; Liu, P.; Wang, H.; Yu, H.; Zhang, S.; Zhu, H.; Peng, F.; Zhao, H. *Langmuir* **2010**, *26*, 1574.
(25) Hosono, E.; Matsuda, H.; Honma, I.; Ichihara, M.; Zhou, H. *Langmuir* **2007**, *23*, 7447.
(26) Reedo, V.; Järvekülg, M.; Lõhmus, A.; Mäeorg, U. *Phys. Status Solidi A* **2008**, *205*, 1511.
(27) Zhang, S.; Peng, L. M.; Chen, Q.; Du, G. H.; Dawson, G.; Zhou, W. Z. *Phys. Rev. Lett.* **2003**, *91*, 256103.
(28) Saupe, G. B.; Waraksa, C. C.; Kim, H.-N.; Han, Y. J.; Kaschak, D. M.; Skinner, D. M.; Mallouk, T. E. *Chem. Mater.* **2000**, *12*, 1556.
(29) Enyashin, A. N.; Seifert, G. *Phys. Status Solidi B* **2005**, *242*, 1361.
(30) Goldberg, D.; Bando, Y.; Eremets, M.; Takemura, K.; Kurashima, K.; Tamiya, K.; Yusa, H. *Chem. Phys. Lett.* **1997**, *279*, 191.
(31) Yasuda, A.; Kawase, N.; Banhart, F.; Mizutani, W.; Shimizu, T.; Tokumoto, H. *J. Phys. Chem. B* **2002**, *106*, 1849.
(32) Menzel, R.; Peiro, A. M.; Durrant, J. R.; Shaffer, M. S. P. *Chem. Mater.* **2006**, *18*, 6059.